Understanding the low-energy incomplete fusion reactions

Abhishek Yadav [ORCID],[1,*] Gobind Ram,[1] M. Shariq Asnain,[2] I. Majeed,[2] Mohd. Shuaib,[2] V. R. Sharma,[3] Indu Bala,[4] U. Gupta,[5]
S. Gupta,[6] D. P. Singh,[7] P. P. Singh,[8] Manoj Kumar Sharma,[9] R. Kumar,[4] B. P. Singh,[2] and R. Prasad[2]

[1]*Department of Physics, Jamia Millia Islamia, New Delhi-110 025, Delhi, India*
[2]*Department of Physics, Aligarh Muslim University, Aligarh-202 002, Uttar Pradesh, India*
[3]*Instituto de Fisica, Universidad Nacional Autonoma de Mexico, Mexico City 04510, Mexico*
[4]*NP-Group: Inter-University Accelerator Centre, New Delhi-110 067, Delhi, India*
[5]*AINST, Amity University, Noida-201 313, Uttar Pradesh, India*
[6]*Department of Physics, Agra College, Agra-282 001, Uttar Pradesh, India*
[7]*Department of Physics, University of Petroleum & Energy Studies, Dehradun-248 007, Uttarakhand, India*
[8]*Department of Physics, Indian Institute of Technology Ropar, Rupnagar- 140 001, Punjab, India*
[9]*Department of Physics, University of Lucknow, Lucknow-226 007, Uttar Pradesh, India*

With a motivation to find out the systematics for the low-energy ($\approx$4–7 MeV/nucleon) incomplete fusion reactions, the experimentally measured excitation functions for evaporation residues, which were populated during the interactions of ^{18}O with ^{159}Tb target nuclei, have been studied. The analysis clearly exhibits that the xn/pxn channels are populated to a large extent through the complete fusion processes. Although, the production cross-section of the α-emitting channels, despite of deducting the precursor decay contribution, found to be significantly under-estimated by the statistical model predictions. The observed enhancement, which may be attributed due to the involvement of break-up fusion processes, is found to be get larger with the incident energy. In addition, the present work in light of the literature data imparts the reliance of incomplete fusion processes on various entrance channel parameters, such as the mass-asymmetry of the interacting partners, fissility parameter and also on the $Z_P Z_T$ (Coulomb factor). These systematics inarguably indicates the projectile type dependency of the incomplete fusion reactions, and the results may be explained on the basis of the α-Q value of the projectile. Furthermore, an attempt has been made to explain the trends of incomplete fusion fractions through the total asymmetry parameter and the system parameter, where system parameter seems to explain the data more satisfactorily, as it incorporates the Coulomb factor as well as the masses of the interacting partners.

I. INTRODUCTION

The quest to understand the reaction dynamics involved in heavy-ion-induced (HI-induced) fusion reactions has always been a topic of great concern, due to its key role in the production and study of the exotic nuclei [1–7]. Fusion is possible for those system where the effective two-body potential must have a pocket called a "fusion pocket," in which the system can be trapped. It is noticed that at energies around the Coulomb barrier (V_b), the "complete fusion" (CF) reactions are the prime contributor to the fusion processes for the medium-mass systems [8–10]. In these reactions, the projectile merges with the target nuclei, for central and/or near central collisions with the influence of strongly attractive nuclear force field (having input angular-momentum window $0 < \ell < \ell_{\mathrm{crit}}$, where ℓ_{crit} is the critical angular-momentum for fusion to occur). However, for peripheral collisions and/or at higher incident energies, the repulsive Coulomb and centrifugal fields become important (fusion pocket vanishes for $\ell > \ell_{\mathrm{crit}}$ in the effective potential-energy curve), and as a con-

sequence the projectile breaks up into its constituent clusters to impart maintainable input angular-momentum to the system, and one of the clusters may amalgamate with the target nuclei to form the reduced excited complex system, certainly, with less mass, charge and excitation energy than the CF [8]. However, the remaining fragments go along almost with the beam velocity and direction [11]. These type of reaction processes termed as the "incomplete fusion" (ICF) reactions. The ICF reactions are specially important to understand because they represent the transition phenomenon between the deep-inelastic and complete fusion reactions with the incident energy.

The existence of direct light particles in the exit channel was proven by Britt and Quinton [12]. However, Alexander and Winsberg [13] were the first to comment on the partial momentum transfer in these events. Furthermore, several models and theories have been proposed to explain these processes, which are generally applicable at energies $\geqslant$10 MeV/nucleon or so [14–24]. But the lack of any adequate theoretical model and/or systematics for the ICF reaction data at low energies (i.e., $\approx$4–7 MeV/nucleon) has triggered a renewed interest in investigating the dynamics of the low-energy breakup reactions.

*abhishekyadav117@gmail.com

In recent years, many attempts have been put forward to understand the low-energy ICF reactions and its sensitivity to various entrance channel parameters [23–35]. Since the establishment of fast α particles in the outgoing channels [12], the first systematic study was performed by Morgenstern *et al.* [14], where the onset and strength of the ICF has been understood on the basis of the entrance channel mass asymmetry, but at relatively higher incident energies $\geqslant 10$ MeV/nucleon. Later on, the projectile-dependent mass-asymmetry systematics, at low energies ($\approx$4–7 MeV/nucleon), has been observed [27]. In several reports the different dependencies of the ICF on the target charge (Z_T) have been reported; in some reports the strength of ICF is independent of Z_T [32]. However, in some it is shown to be almost proportional to Z_T [10,30,31]. Apart from this, in one of our papers, the sensitivity of the low-energy ICF reactions on the projectile structure, through the α-Q value (energy needed to detach an α particle from the projectile) of the projectile have been emphasized [33]. In another work, how $Z_P Z_T$ (Coulomb factor) affects the ICF strengths has been studied [34]. It is not out of place to mention that the limitations of the proposed $Z_P Z_T$ systematics [34] has been highlighted in one of our recent papers [35].

Furthermore, in some very recent efforts, the dependence of the low-energy ICF reactions on few more entrance channel parameters, such as the neutron thickness, neutron excess in the target $(N - Z)_T$, deformation of the target nuclei (β_2^T), deformation length ($\beta_2^T R_T$), interaction radius (R_T), and combinations of these as; $Z_P Z_T \beta_2^T$, $Z_P Z_T / (1 - \beta_2^T)$, $\mu \beta_2^T$, etc., have been introduced without much explanations and/or their intercorrelations with other entrance channel parameters [36–40]. It is not out of place to mention that more systematic efforts are required to understand the low-energy ICF reactions.

As a consequence, in the present work, the measurement and analysis of the excitation functions (EFs) of the evaporation residues (ERs), originated in the interactions of ^{18}O with ^{159}Tb at energies $\approx 1.01 V_b$ to $1.42 V_b$ (V_b, the fusion barrier of the system $\approx$69.75 MeV), have been performed. To draw some systematics and to delve in the possible aspects of the low-energy ICF reactions, the present data have been compared with the literature data available for other sizable number of projectile-target combinations ($\approx$44) with wide range of $Z_P Z_T$ values ($\approx$138–670).

The present paper is structured as follows: the experimental details are given in Sec. II, while Sec. III is dealing with the details of the measurements and results, Sec. IV is discussing the reliance of the ICF reactions on different entry state parameters, and finally the summary is presented in Sec. V.

II. EXPERIMENTAL DETAILS

The experiments have been carried out at the Inter-University Accelerator Centre (IUAC), New Delhi, to study the EFs of the fusion evaporation residues, produced in the interactions of ^{18}O (a nonalpha clustered beam) on a ^{159}Tb target. The activation technique along with off-line γ-ray spectroscopy have been used. Isotopically pure, self-supporting targets of ^{159}Tb (target thickness $t_m \approx 0.98$–2.00 mg/cm^2) and the aluminum catcher and energy

degrader foils ($t_m \approx 1.6$–2.6 mg/cm^2) have been prepared by rolling technique. The thickness and uniformity of the target and catcher foils have been determined prior to use to an accuracy of 1%, by measuring the energy lost in traversing the foil by 5.49 MeV α particles from an ^{241}Am source, and using the values of the stopping power from the SRIM code [41]. To obtain the EFs measurements for wide energy range, the energy degradation technique have been used. In this method after each target foil, an Al-catcher foil of adequate thickness is placed, this arrangement hereafter called the target-catcher foil assembly. Here, the Al-catcher foil fulfill two objectives; stopping the heavy recoils populated during the bombardments in their respective target-catcher foil assembly, and also lowering the incident-beam energy for the next target-catcher foil assembly. In the present experiment, four stacks have been prepared, each stack having three target-catcher foil assemblies. These stacks have been irradiated at four different bombarding energies viz., $\approx$82, 95, 97, and 100 MeV in the general purpose scattering chamber (GPSC) [42] for $\approx$8–10 hour duration, according to the half-lives of the expected residues populated during the interactions. To monitor the beam current, which was maintained $\approx$25–30 nA during all the irradiations, a Faraday cup at the beam dump has been used.

Furthermore, after each irradiation, to record the induced activity in each target-catcher foil assembly, the irradiated stacks have been taken out of the GPSC using the in-vacuum transfer facility to minimize the gap between the stop of irradiation of the samples to the start of the counting of the induced activity [42]. After being taken out, the stacks were dismantled carefully, and a precalibrated high-resolution HPGe detector has been used to record the induced radio-activities in the target-catcher foils. The CAMAC-based data-acquisition system has been used [43]. Several rounds of counting, for all the target-catcher foil assemblies, have been carried out, initially for the short time span (i.e., $\approx$100–300 s) to catch the short-lived reaction products, and then for long durations (i.e., $\approx$10–60 minutes) to identify relatively long-lived reaction products. The calibration of the HPGe detector, and the efficiency of the detector at various source-detector separations at which the counting of irradiated samples were performed, have been measured using the standard γ-ray sources, like ^{60}Co or ^{152}Eu. The energy resolution of the detector has been estimated to be 2.0 keV for the 1.33 MeV γ line of a ^{60}Co source. The data analysis methodology and interpretation of the results are discussed in the following sections.

III. DATA ANALYSIS AND RESULTS

In the present work, to measure the EFs of the residues produced during the interactions of ^{18}O + ^{169}Tm system, the identification of the reaction products have been achieved using their characteristic decay γ lines in the recorded γ-ray spectra and by examining their decay curves. In Fig. 1, a part of the recorded γ-ray spectrum obtained at incident energy 91.28 ± 0.44 MeV is shown, where some of the γ lines correlated to the different reaction products have been labeled. As a typical example, the decay curve of ^{174}Ta ($t_{1/2} = 1.05$ h) residues has also been shown in the inset of the Fig. 1, which
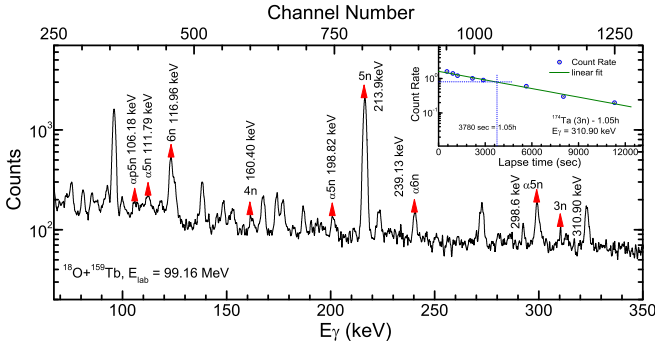
FIG. 1. As a representative case, a typical γ-ray spectrum acquired for $^{18}O + ^{159}Tb$ interactions at 91.28 ± 0.44 MeV beam energy, where different CF and/or ICF residues have been identified based on their characteristic γ lines and by analyzing their decay curves. For example, the decay curve of ^{174}Ta ($t_{1/2} = 1.05$ h) residues populated via $3n$-channel has been shown in inset (see text for details).

is in good agreement with the literature value of its half-life, as a result confirms the identification of ^{174}Ta residues. Similar methodology has been followed to identify the other ERs. Furthermore, the production cross sections of all the identified ERs have been calculated using the standard formulation [44]. In the present work, attempts have been made to minimize the errors in the production cross sections of measured radionuclides. The errors can arise from variety of sources, such as (*i*) the nonuniformity of the target foils, which may lead to the uncertainty in estimating the number of target nuclei in the sample. However, to ensure the uniformity of the target foils, thickness of each sample was measured at different positions by the α-transmission method, and the error in the thickness estimation may be $\approx 1\%$. (*ii*) Uncertainty in incident flux estimation, i.e., fluctuations in the beam current, and thus proper care has been taken to maintain the beam current constant, and variations in the beam current during the irradiations, if observed, have been noted down so that the error due to beam current fluctuations may be minimized. (*iii*) Uncertainty in determining the geometry-dependent efficiency of the gamma spectrometer, and the error in the efficiency determination, due to the statistical fluctuations in counts, is estimated to be less than 2%. (*iv*) The dead time of the spectrometer was kept minimum by suitably adjusting the source-detector distance, also, to properly estimate the dead time of the detector, a 50 Hz pulser has been used. In the present study, attempts have been made to reduce the uncertainty caused by all of the aforementioned factors, and the cumulative error including statistical errors is estimated to be $\leqslant 15\%$, excluding the uncertainty in branching ratio, decay constant, etc.

Furthermore, in the recorded γ-ray spectra, all the γ lines except the background activity could not be designate to any of the CF and ICF residues, thus the origin of these unassigned γ lines could be from some other possible reaction processes, for example, the fission of the composite system which formed through CF and/or ICF processes, because this process has finite probability at these energies and mass region [45].

TABLE I. The spectroscopic properties of the observed reaction residues, for which the EFs have been measured.

Residue	$T_{1/2}$	J^π	E_γ (keV)	I^γ (%)
$^{174}Ta(3n)$	1.05 h	3^+	206.50	57.7
			310.90	1.06
$^{173}Ta(4n)$	3.14 h	$5/2^-$	160.40	4.8
			172.19	17.0
$^{172}Ta(5n)$	36.8 min	3^+	213.96	52.0
$^{171}Ta(6n)$	23.3 min	$5/2^-$	116.96	5.5
			166.3	19.2
$^{171}Lu(\alpha 2n)$	8.24 days	$7/2^+$	667.4	11.06
			739.8	48.0
$^{168}Lu^g(\alpha 5n)$	5.5 min	$6^{(-)}$	111.79	49[a]
			228.58	70[a]
$^{168}Lu^m(\alpha 5n)$	6.7 min	3^+	198.82	28
			884.64	13.9
$^{167}Lu(\alpha 6n)$	51.5 min	$7/2^+$	239.32	8.6
$^{167}Yb(\alpha p5n)$	17.5 min	$5/2^-$	113.34	55.4
			106.18	22.6

[a]These intensities are relative.

In the present work, the EFs of $^{174}Ta(3n)$, $^{173}Ta(4n)$, $^{172}Ta(5n)$, $^{171}Ta(6n)$, $^{171}Lu(\alpha 2n)$, $^{168}Lu(\alpha 5n)$, $^{167}Lu(\alpha 6n)$, and $^{167}Yb(\alpha p5n)$ radionuclides populated in the interactions of $^{18}O + ^{159}Tb$ system, have been measured for the energy range $1.01V_b–1.42V_b$ and, are tabulated in Table I, with their spectroscopic signatures taken from Refs. [46,47]. Furthermore, in order to understand the production mechanism and course of cross-section for the identified reaction products, the experimentally measured EFs have been reviewed within the framework of one of the widely used statistical model code PACE4 [48,49]. The details of the code are given in Refs. [44,48,49]. For ready reference a brief account of the same is given here; as a fusion reaction is termed as a reaction, which forms a compound nucleus (CN), the concept of which was originally proposed by Niels Bohr in 1936 [50]. Thus, the basis of this code is the equilibrated CN-decay of the Hauser-Feshbach theory [51]. This code uses the statistical approach of CN deexcitation by Monte Carlo procedure and the angular-momentum projections are calculated at each stage of the deexcitation, which enables the determination of the angular distribution of the emitted particles. In this code the angular-momentum conservation is taken into account. This code has been modified to take into account the excitation energy dependence of the level-density parameter using the prescription of Kataria *et al.* [52]. The default optical model parameters for the neutrons, protons, and the α particles were used [48]. The γ-ray strength functions for $E1$, $E2$, and $M1$ transitions were taken from the tables of Endt [53]. In this code, the level-density parameter ($a = A/K$ MeV^{-1}, where A is the mass number of the nucleus and K is a free adjustable parameter) is one of the important parameters. The BASS model is used to calculate the CF cross sections [54]. The value of the free parameter K may be varied to reproduce the experimentally measured EFs, and also to understand the production mechanism of the reaction products. It may, however,
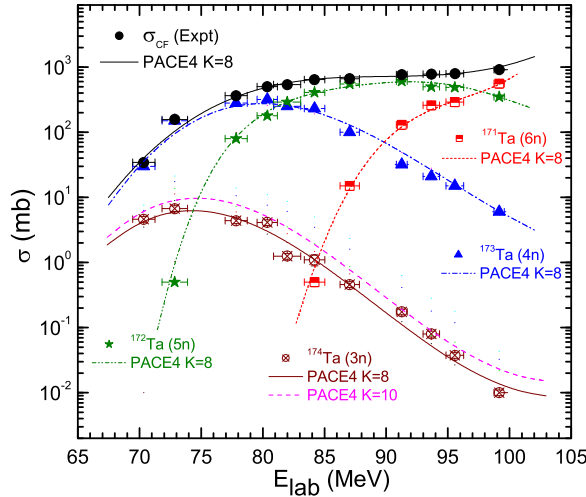
FIG. 2. Experimentally measured EFs of ^{174}Ta($3n$), ^{173}Ta($4n$), ^{172}Ta($5n$), and ^{171}Ta($6n$) residues populated in the ^{18}O + ^{159}Tb interactions. Self explanatory notations have been used. The lines through the data points are predictions done using the PACE4-code (see text for details).

be pointed out that the breakup and pre-equilibrium processes are not taken into consideration in this code.

A. Analysis of the *xn/pxn* channels

In view of the fact that the comparison of the experimental and theoretical EFs of the reaction products may signals about the associated reaction mechanism in their production, and, hence, the appropriate values of the input parameters used in the prediction of the EFs using the statistical model code is an essential part of the analysis. In the present work, the EFs of residues ^{174}Ta, ^{173}Ta, ^{172}Ta, and ^{171}Ta, likely to be originated, respectively, via $3n$, $4n$, $5n$, and $6n$ emission from the excited ^{177}Ta* composite nucleus, have been measured experimentally and the same have been plotted in Fig. 2. It is not out of place to mention that none of the *pxn* channels could be observed in the present work may be due to their short or long half-lives.

Furthermore, to understand the involved reaction mechanism in the origin of these reaction products, the theoretical EFs have been modeled through the statistical code PACE4. In this code, the value of the free parameter K is varied, with in the physically justified limits. As reported by Gilbert and Cameron in their level-density systematics, the values of the free parameter K significantly higher than $K = 10$ are implausible for the excitation energy and mass region of current interest [55]. Furthermore, during the comparison of experimentally measured EFs with that of the theoretical ones, the enhancement observed, if any, over the PACE4 predictions may be ascribed to some physical effects which were not considered in this code. Now, as can clearly be noticed from the Fig. 2 that the experimental EFs of these *xn* channels are in good agreement, throughout the studied energy range, with the calculations done through the statistical model PACE4 for the level-density value $a = A/8$ MeV^{-1}. This satisfactory agreement between the experimental and theoretical EFs leads to the following conclusions: first is that the origin of these
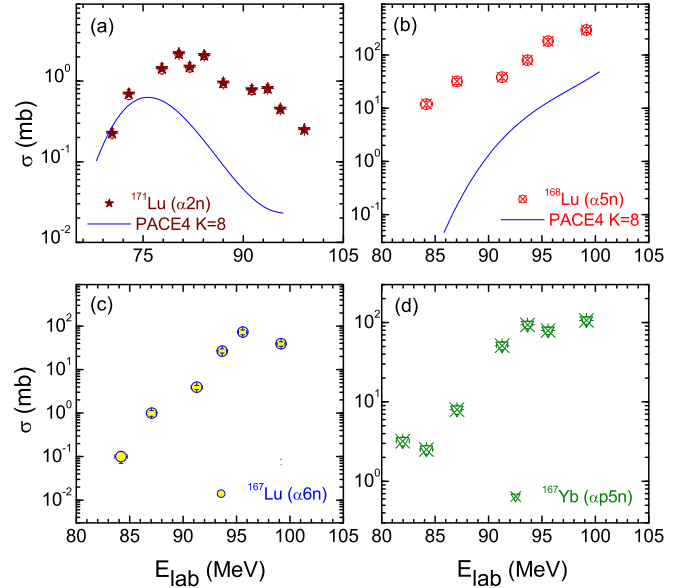

FIG. 3. The comparison of the experimental and theoretical EFs of α-emitting channels. The symbols are the experimental data points and the solid blue curves represent the PACE4 predictions (see text for the details).

residues (*xn* channels) are through the deexcitation of the fully equilibrated compound nucleus (^{177}Ta*) formed via complete fusion of ^{18}O with ^{159}Tb target nuclei, and second, this reproduction also validates the choice of the parameters used for the analysis. Thus, this allows us to use the same set of parameters, uniformly, for further analysis.

B. Analysis of the α-emitting channels

In the present work, the EFs of the following α-emitting channels: ^{171}Lu($\alpha2n$), ^{168}Lu($\alpha5n$), ^{167}Lu($\alpha6n$), and ^{167}Yb($\alpha p5n$), populated during the interactions of ^{18}O with ^{159}Tb targets, have been measured. And to make a comparison of the measured EFs with the estimated through the statistical code, to understand the reaction mechanism involved in their production, both are plotted in Figs. 3(a)–3(d). In these plots the symbols are the experimental cross sections of these residues and the solid blue curves are the estimates of the PACE4 code for level-density value $a = A/8$ MeV^{-1}. These PACE4 calculations were performed with the same set of parameters as used to understand the EFs of the *xn* channels.

As can be noticed from Fig. 3(a), the experimental cross sections for the residues ^{171}Lu match with the theoretical calculations at low energies; however, as energy increases, the cross sections are enhanced over the PACE4 predictions. And for the ^{168}Lu residues, the experimental cross sections are quite large compared with the PACE4 estimations in the entire range of energy under investigation. However, there were negligible theoretical estimates for residues ^{167}Lu and ^{167}Yb, and thus not shown in Figs. 3(c)–3(d). As a result, these two radionuclides (^{167}Lu and ^{167}Yb) are purely populated via ICF processes; however, the enhancement in the cross sections for ^{171}Lu and ^{168}Lu residues may be attributed to the ICF reactions since the code PACE4 does not include the breakup

reactions. Thus, it may be culminated that the population of these residues (α-emitting channels) may have contributions from both the CF and/or ICF reaction processes. For example, the evaporation residue ^{171}Lu can have contributions through the following routes:

(i) CF: the entire projectile ^{18}O fuses with the target ^{159}Tb, forming the composite system ^{177}Ta and then, after attaining equilibrium, emits $\alpha 2n$ and forms ^{171}Lu residues:

$$^{18}O + {}^{159}Tb \Rightarrow {}^{177}Ta^* \Rightarrow {}^{171}Lu + \alpha 2n.$$
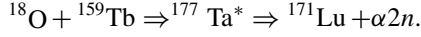
(ii) ICF: when only a part of the projectile ^{18}O (e.g., ^{14}C) fuses with the target ^{159}Tb to form an incompletely fused composite system (in this case ^{173}Lu*), and the remaining α particle flows in the beam direction with out interaction. Thus formed composite system ^{173}Lu* may decay by evaporating two neutrons ($2n$), consequently, populating the same residue ^{171}Lu:

$$^{18}O({}^{14}C + \alpha) \Rightarrow {}^{14}C + {}^{159}Tb \Rightarrow {}^{173}Lu^* \Rightarrow {}^{171}Lu + 2n,$$
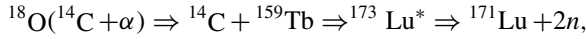
where the α-particle is a spectator.

Similarly, the other α-emitting channels may also be populated via both the CF and/or ICF reaction processes. It is not out of place to mention that residues ^{167}Lu and ^{167}Yb populated via $\alpha 6n$ and $\alpha p 5n$, respectively, have negligible contribution from the CF processes. Thus, these residues are mainly populated via ICF reaction processes. It can clearly be noticed from Fig. 3 that the weighting of the ICF processes, in these residues, depends on energy. Hence, the ICF contributions, in the production of the observed $\alpha xn/\alpha pxn$ channels have been deduced by subtracting the PACE4 predictions for $\alpha xn/\alpha pxn$ channels from their corresponding experimental cross sections at each studied energy, i.e., the ICF cross section at an energy "ϵ" is deduced through $\Sigma \sigma_{\alpha xn + \alpha pxn}^{expt}(\epsilon) - \Sigma \sigma_{\alpha xn + \alpha pxn}^{PACE4}(\epsilon) = \sigma_{ICF}(\epsilon)$.

C. Incomplete fusion strength function

For better understanding about the emergence and influence of the ICF processes, the contribution of the ICF reactions to the total fusion cross section have been deduced as the percentage fraction of ICF at an energy (say, ϵ), and is defined as $\%F_{ICF}(\epsilon) = [\Sigma \sigma_{ICF}(\epsilon)/\sigma_{TF}(\epsilon)] \times 100\%$; where $\sigma_{TF}(\epsilon) = \Sigma \sigma_{CF}(\epsilon) + \Sigma \sigma_{ICF}(\epsilon)$.

It is worth mentioning that the ICF strength deduced in our earlier measurements of the EFs for some systems nicely matches with that obtained from the analysis of the forward ranges (RRDs) and angular distributions (ADs) of heavy recoils for those same systems [56–58]. It is important to note that, in these measurements of RRDs and ADs, the CF and ICF events are identified distinctly through full and partial linear momentum transfer components, respectively, which were measured unambiguously in these measurements, experimentally, and consequently the deduced ICF contributions are independent of the statistical model predictions in both these measurements (RRDs and ADs) [56–58]. Furthermore, as already put forward that the α-emitting channels may have originated via both the CF and/or ICF processes, and because
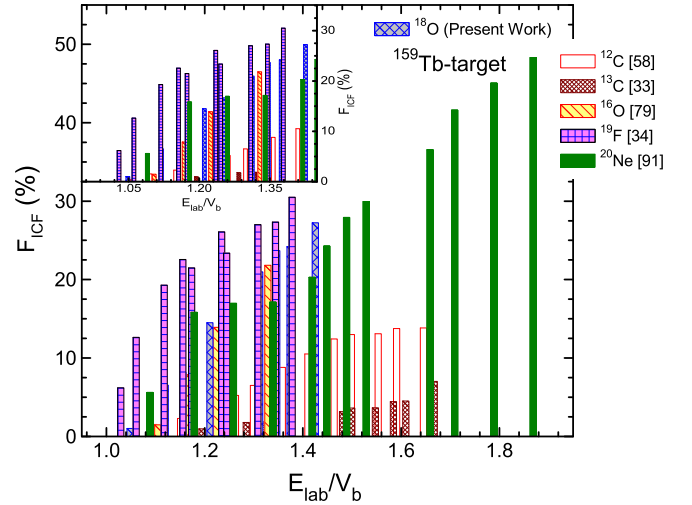

FIG. 4. To see the reliance of the projectile type, the F_{ICF} strengths for several system, different projectiles on the same targets ^{159}Tb, have been compared, and the x axis is normalized by their corresponding Coulomb barriers. For better visualization at low energies, the zoomed version of the same is shown in the inset (for details see text).

of this, in the measurements of RRDs and ADs [56–58], the weights of the CF cross section in α-emitting channels are satisfactorily matches with the PACE4 simulations done with the same set of parameters as used to estimate the production cross section of the xn/pxn channels. This reproduction of the CF contribution in the α-emitting channels gives credence to the choice of the PACE4 parameters. Also, the satisfactory agreement in the values of ICF fractions, deduced from two independent measurements, corroborate the analysis and method of deducing the ICF contribution, as well as the selection of the parameters used in estimating the theoretical cross sections.

Hence, in order to study the reliance of the ICF reaction mechanism on the projectile type, the deduced F_{ICF} values for the present system along with other systems, with different projectiles on the same target ^{159}Tb, have been plotted in Fig. 4. The effect of the various entrance channel parameters on the ICF-reaction dynamics will be discussed in the following sections.

IV. HOW IS INCOMPLETE FUSION INFLUENCED BY DIFFERENT PARAMETERS?

A. Role of incident beam energy

As has been discussed that the ICF reactions occur for the input angular-momentum values above the critical angular momentum (ℓ_{crit}) for fusion, and the incident-beam energy is one of the ways to impart the input angular-momentum to the system, and hence it is important to understand the sensitivity of the ICF reaction processes on the same. The F_{ICF} values have been plotted in Fig. 4 with respect to the normalized projectile energy to counterbalance the results of different Coulomb barriers.

Now, the following facts can clearly be noticed from this figure in one go: (i) the value of F_{ICF} increases with the incident-beam energy for all the systems, (ii) the rate of change of F_{ICF} values are different for the different projectile-target combinations. Since the target nuclei is same for these systems, thus it can be inferred that the F_{ICF} values are sensitive to the projectile type, (iii) the threshold energy, the onset energy for the ICF, is also different for each system.

In detail, as can be seen from Fig. 4, for the presently studied system $^{18}O + ^{159}Tb$, the value of F_{ICF} is found to be $\approx 0.60\%$ at incident energy $1.04V_b$ and the ICF strength increases smoothly up to $\approx 27.24\%$ at the highest measured energy (i.e., $1.42V_b$). Largely similar behavior of the F_{ICF} values with the incident energy have been observed for the other systems as well. The most suitable explanation for these observations is that, as the incident energy increases, it brings larger input angular momentum to the system, consequently, the depth of the fusion pocket in the effective potential-energy curve is reduced. Thus, the projectile breaks up into its constituents, certainly, to provide the sustainable input angular momenta to the system and, of course, to restore the fusion pocket, which may lead to the fusion of one part of the projectile with the target nucleus, resulting in the ICF reaction processes. As an example some of the breakup combinations that may be observed in the ^{18}O-induced reactions are (i) ^{18}O may break up into ^{14}C and ^{4}He clusters, (ii) ^{10}Be and $2\,^{4}He$ fragments, and/or (iii) four α particles along with two neutrons. Hence, matching input angular-momentum conditions for different fragment-target combinations, leads to the ICF reaction processes.

Further, as in Fig. 4, the F_{ICF} curves are different for the different projectiles on the same target ^{159}Tb, which concludes that the F_{ICF} values are also sensitive to the projectile type. A thoughtful observation suggests that the values of F_{ICF} for ^{19}F, ^{18}O (nonalpha clustered projectiles) are large than the well-known alpha-clustered projectiles ^{20}Ne, ^{16}O, ^{12}C, throughout the studied energy range. However, in contrast, the ^{13}C projectile (being the nonalpha clustered) shows different trend, that is the magnitudes of ICF fractions, for ^{13}C, are smaller than the other projectiles.

Furthermore, it may also be pointed out from the same figure that the threshold energy ($E_{th_{ICF}}$ energy at which the ICF starts), similar to the magnitude of F_{ICF}, is also depends on the type of the projectile. For the ^{18}O as projectile, the onset of ICF appears to be relatively at lower energy (i.e., $E_{th_{ICF}}^{18_O} \approx 1.04V_b$) than for the ^{16}O ($E_{th_{ICF}}^{16_O} \approx 1.07V_b$) induced reactions with ^{159}Tb targets. The ICF's emergence energy for ^{20}Ne, ^{19}F, ^{13}C, and ^{12}C projectiles may be $E_{th_{ICF}}^{20_{Ne}} \approx 1.07\,V_b$, $E_{th_{ICF}}^{19_F} \approx 1.04\,V_b$, $E_{th_{ICF}}^{13_C} \approx 1.21\,V_b$, and $E_{th_{ICF}}^{12_C} \approx 1.12\,V_b$, respectively. From these observations, it can be concluded that the ^{19}F, among all these projectiles, has the smallest threshold energy at which the ICF assumed to be started. Similar observations have been noticed for the other targets, as well. Hence, from all these observations; different F_{ICF} values for different projectile, different onset energy, etc., it is culminated that some property linked to the structure of the projectile (viz., binding energy, Q_α value, shape of the nuclei, etc.), other than the cluster nature, also influenced the ICF reaction dynamics.
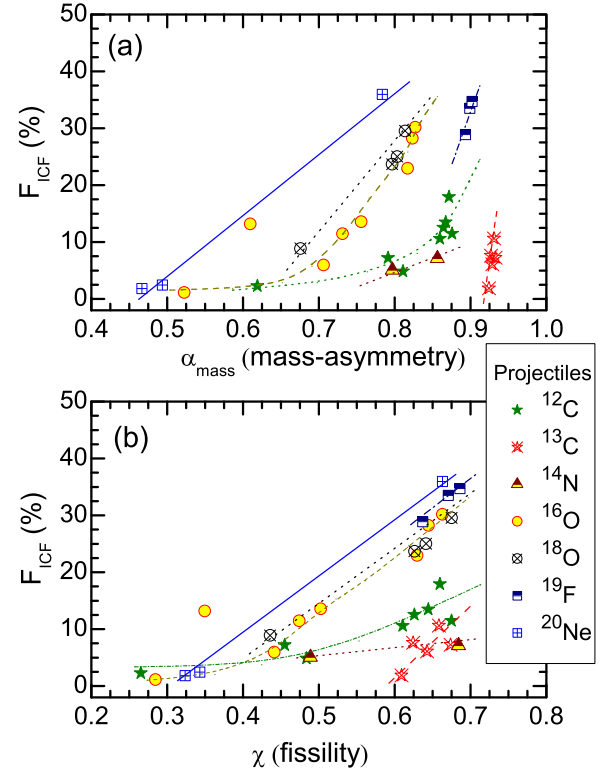

FIG. 5. The incomplete fusion fraction F_{ICF} for various systems have been compared, at a constant E_{lab}/V_b value, in terms of (a) the mass asymmetry (α_{mass}) of the interacting partners, and (b) the fissility parameter (χ). The lines are just to guide the eyes (see text for explanation).

B. Role of mass asymmetry α_{mass}

Since the very beginning of the heavy-ion fusion reaction studies, the impact of the entrance channel mass asymmetry [$\alpha_{mass} = (A_T - A_P)/(A_T + A_P)$] degree of freedom on reaction mechanism have been studied [59,60]. After the first observation of the fast alpha-particle in the exit channel by Brit and Quinton [12], which was explained by the breakup of the projectile, Morgenstern *et al.* observed a correlation between the onset and the strength of the ICF reactions at high energies, $\geqslant 10$ MeV/nucleon, to the α_{mass} of the interacting partners, which states that the ICF reactions contribute significantly for the increased mass asymmetry of the systems [14]. Hence, in order to strengthen the understanding and to extend the entrance channel mass-asymmetry systematics to the low-energy ICF data, the F_{ICF} values obtained for the present system, along with the data available for the other systems tabulated in Table II, have been examined in light of the Morgenstern's mass-asymmetry systematics at constant normalized beam energies. As a representative case the F_{ICF} values at $E_{lab}/V_b = 1.35$, for all systems, have been presented in Fig. 5(a). The following points may be noticed from this figure: first, the ICF fraction increases with recognizably different trends for each projectile, with the mass asymmetry of the interacting partners. Second, the F_{ICF} values are significantly different for the same mass asymmetric systems. These observations are in contrary to the Morgen-

TABLE II. List of systems, and their entrance channel parameters, used for the systematic study. Here, $Z_P Z_T$, the product of the atomic numbers of the interacting partners, α_{mass}, the mass-asymmetry, α_{total}, the total asymmetry, χ, the fissility parameter, and ζ, the system parameter. The different systems with same $Z_P Z_T$ values are marked by A, B, C, etc.

System	E/V_b	$Z_P Z_T$	α_{mass}	α_{total}	χ	ζ	Ref.
^{12}C +							
^{51}V	1.3–2.61	138	0.6190	0.3629	0.2653	430.11	[61]
^{52}Cr	2.0–3.35	144	0.6250	0.3750	0.2783	449.64	[62]
^{59}Co	2.15–2.86	162^A	0.6620	0.4213	0.3041	511.57	[63]
^{103}Rh	1.26–2.09	270	0.7913	0.6051	0.4549	885.16	[64]
^{115}In	1.28–1.98	294	0.8110	0.6341	0.4836	969.14	[65]
^{159}Tb	1.12–1.67	390^E	0.8596	0.7144	0.6107	1302.73	[58]
^{165}Ho	1.08–1.64	402^F	0.8644	0.7223	0.6259	1344.53	[66]
^{169}Tm	1.08–1.63	414^G	0.8674	0.7286	0.6445	1385.78	[67]
^{175}Lu	1.04–1.57	426^H	0.8717	0.7358	0.6597	1427.57	[68]
^{181}Ta	1.07–1.40	438^I	0.8756	0.7426	0.6751	1469.35	[69]
^{13}C +							
^{93}Nb	1.70–2.33	246^B	0.7547	0.5620	0.4191	830.80	[70]
^{159}Tb	1.21–1.69	390^E	0.8488	0.7054	0.6090	1351.98	[33]
^{165}Ho	1.07–1.64	402^F	0.8539	0.7136	0.6243	1395.50	[71]
^{169}Tm	1.19–1.58	414^G	0.8571	0.7200	0.6428	1438.40	[72]
^{175}Lu	1.05–1.58	426^H	0.8617	0.7274	0.6582	1481.91	[68]
^{181}Ta	1.08–1.41	438^I	0.8660	0.7344	0.6736	1525.40	[69]
^{14}N +							
^{124}Sn	1.32–1.71	350	0.7971	0.6013	0.4891	1241.38	[37]
^{169}Tm	1.02–1.28	483^C	0.8470	0.6910	0.6537	1736.72	[73]
^{175}Lu	1.00–1.34	497	0.8519	0.6990	0.6690	1789.40	[28]
^{181}Ta	0.98–1.31	511	0.8564	0.7065	0.6843	1842.07	[29]
^{16}O +							
^{45}Sc	1.35–3.45	168^A	0.4754	0.2131	0.2721	577.18	[74]
^{51}V	1.37–2.82	184	0.5224	0.2528	0.2847	642.13	[75]
^{66}Zn	1.47–2.25	240	0.6098	0.3530	0.3494	861.26	[76]
^{74}Ge	1.16–2.15	256^B	0.6444	0.3867	0.3572	928.53	[74]
^{93}Nb	1.37–1.96	328	0.7064	0.4758	0.4409	1211.89	[77]
^{103}Rh	1.21–1.53	360	0.7311	0.5104	0.4740	1339.70	[44]
^{115}In	1.14–1.83	392	0.7557	0.5436	0.5025	1469.13	[78]
^{148}Nd	1.02–1.52	480^C	0.8049	0.6155	0.5845	1823.94	[36]
^{159}Tb	1.07–1.35	520	0.8171	0.6380	0.6293	1982.64	[79]
^{165}Ho	1.02–1.47	536	0.8232	0.6476	0.6445	2047.05	[80]
^{169}Tm	1.02–1.29	552	0.8270	0.6552	0.6630	2110.36	[79]
^{175}Lu	1.06–1.32	568	0.8325	0.6639	0.6783	2174.76	[81]
^{181}Ta	1.00–1.30	584^D	0.8376	0.6721	0.6936	2239.13	[82]
^{18}O +							
^{93}Nb	1.21–1.94	328	0.6757	0.4550	0.4358	1273.77	[83]
^{159}Tb	1.01–1.42	520	0.7966	0.6220	0.6259	2090.99	a
^{165}Ho	1.10–1.46	536	0.8033	0.6319	0.6413	2159.32	[84]
^{175}Lu	1.02–1.33	568	0.8135	0.6487	0.6751	2294.69	[85]
^{19}F +							
^{159}Tb	1.04–1.39	585^D	0.7865	0.5952	0.6369	2410.02	[34]
^{169}Tm	0.97–1.27	621	0.7979	0.6137	0.6706	2566.45	[86]
^{175}Lu	1.01–1.30	639	0.8041	0.6232	0.6859	2645.43	[87]
^{20}Ne +							
^{51}V	1.84–3.22	230	0.4366	0.1720	0.3041	871.76	[88]
^{55}Mn	1.08–3.44	250^B	0.4667	0.2000	0.3236	957.43	[89]
^{59}Co	1.26–3.00	270	0.4937	0.2268	0.3430	1043.50	[90]
^{159}Tb	1.07–1.85	650	0.7765	0.5695	0.6479	2739.68	[91]
^{165}Ho	1.06–1.82	670	0.7838	0.5802	0.6630	2829.74	[92]

^{a}Present work.

stern's mass-asymmetry systematics [14], and thus suggests the "projectile-dependent mass-asymmetry" systematics.

There are several systems available with almost matching entrance channel mass-asymmetry α_{mass}, and for ready reference few are mentioned here: (i) $^{18}O + ^{159}Tb$ (0.7966), $^{14}N + ^{124}Sn$ (0.7971), and $^{19}F + ^{169}Tm$ (0.7979), (ii) $^{12}C + ^{93}Nb$ (0.7714), $^{16}O + ^{124}Sn$ (0.7714), and $^{20}Ne + ^{159}Tb$ (0.7765), (iii) $^{13}C + ^{93}Nb$ (0.7547), and $^{16}O + ^{115}In$ (0.7557), (iv) $^{16}O + ^{74}Ge$ (0.6444), $^{20}Ne + ^{93}Nb$ (0.6460), and $^{16}O + ^{75}As$ (0.6484), etc. All these projectile-target combinations have almost matching mass asymmetry of the interacting partners, but there is a significant difference in the values of F_{ICF} have been observed for the entire studied energy range. Also, it can be noticed from this figure that the trend of the F_{ICF} are different for individual projectiles, which reflects that the projectile structure, together with the mass asymmetry of the interacting partners, plays an important role in understanding the ICF-reactions at energies just above the Coulomb barrier.

C. Role of fissility parameter χ

The presence of the ICF reactions, along with other reaction processes like fission, quasifission, etc., may add up the complexity to synthesize the superheavy elements [1–7]. In the present work, one of the prime experimental assignments is to understand the dependence of these (ICF reactions) processes on the properties of the interacting partners and, of course, to identify the trends which can be summarized into a systematics. Hence, in order to understand, the role of the fissility parameter on the ICF reactions, the F_{ICF} values at a constant normalized projectile energy ($E_{lab}/V_b = 1.35$), for different projectile-target combinations have been plotted against the fissility parameter in Fig. 5(b). Fissility is a parameter expressing the stability of the charged liquid drops. Fissility is a very useful concept first introduced by Lord Rayleigh [93], and later this liquid drop model (LDM) was adapted by Niels Bohr to the atomic nuclei and derived the theory of nuclear fission [94].

It may clearly be noticed from Fig. 5(b) that F_{ICF} increases with the fissility parameter for each individual projectiles, and these trends seems similar to the mass-asymmetry parameter dependency of the ICF reactions. It is not out of place to mention that both these systematics, mass asymmetry and fissility, represents a strong projectile-type dependency, i.e., different F_{ICF} trend for each projectile, thus, the projectile structure along with these parameters may play an important role in the ICF-reactions at these low energies.

D. Role of projectile's α-Q value

In ICF reactions, it is assumed that the projectile nucleus breaks up into its constituent fragments in the nuclear field of the target nucleus and a fragment of the incident nucleus fuses with the target nucleus to form a partially fused composite system. If this is the case, then the projectile with less binding energy per nucleon is likely to show larger ICF contribution. However, from Fig. 4, the projectile ^{20}Ne ($E_b \approx 8.03$ MeV) with the largest magnitude of
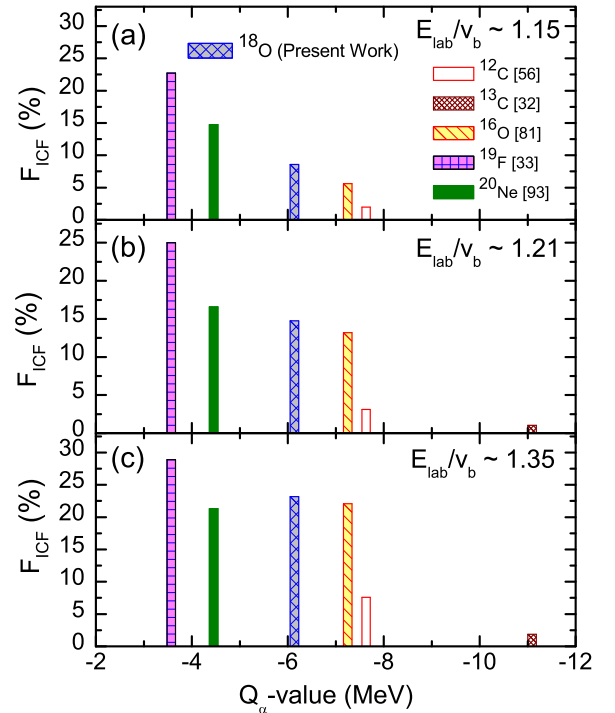

FIG. 6. The incomplete fusion fraction F_{ICF} for systems, with different projectiles on the same target ^{159}Tb, compared in terms of the Q_α value of the projectile at three different E_{lab}/V_b values; (a) 1.15, (b) 1.2, and (c) 1.35 (see text for the explanation).

binding energy per nucleon as compared with ^{18}O ($E_b \approx 7.77$ MeV), ^{16}O ($E_b \approx 7.98$ MeV), ^{13}C ($E_b \approx 7.47$ MeV), and ^{12}C ($E_b \approx 7.68$ MeV), is showing higher magnitudes of ICF fractions than other projectiles. Thus, the binding energy per nucleon of the projectile does not seem to make any noteworthy contribution to ICF reactions.

Furthermore, an entrance channel parameter, the projectile's α-Q value (Q_α), which is expressed as the minimum energy needed to eject an α particle from the projectile, have been considered to understand these observations regarding the strong projectile-type effect on ICF reactions. The Q_α values for the projectiles ^{20}Ne, ^{19}F, ^{18}O, ^{16}O, ^{13}C, and ^{12}C are -4.72, -4.01, -6.22, -7.16, -10.64, and -7.36 MeV, respectively. Thus, to understand the trends of Figs. 4, and 5, the ICF fraction have been plotted as function of projectile's Q_α value, at constant E_{lab}/V_b, for different projectiles on the same target ^{159}Tb, keeping the target ambience same, and for better representation three cases are shown in Figs. 6(a)–6(c). These figures clearly reflect that the ICF strength function depends on the Q_α value of the projectile. As can be seen from Fig. 6(a), the ^{19}F projectile with the smallest magnitude of Q_α value (-4.01 MeV) has the largest magnitude of the F_{ICF} ($\approx 23\%$), and at the same $E_{lab}/V_b \approx 1.15$ value, the ^{13}C with the greatest Q_α-value magnitude (-10.64 MeV) seems to have no incomplete fusion contribution, while ^{12}C with a Q_α value of -7.36 has $\approx 1.97\%$ ICF contribution. Thus, the ICF strength function increases with the Q_α value of the projectile. Similar observations have been noticed at other $E_{lab}/V_b \approx 1.2$, and 1.35 values. It can also be noticed that at

$E_{lab}/V_b \approx 1.35$, the F_{ICF} value for ^{20}Ne is less compared with ^{18,16}O as projectile, being the less negative Q_α value projectile as compared with ^{18,16}O.

Furthermore, it is not out of place to mention that the weight of the Q_α value is not the same at all incident energies, as different increasing trends of F_{ICF} with Q_α value can clearly be seen in Figs. 6(a)–6(c). To understand this observation more clearly, this systematics have been checked for other projectile-target combinations, and similar observations have established the above findings. Thus, it can certainly be pointed out that the Q_α value of the projectile is one of the important parameter, which influences the breakup probability of the projectile and hence contribute significantly to interpret the low-energy ICF-reactions.

E. Role of Coulomb factor $Z_P Z_T$

It can indubitably be shown that the increase in the Coulomb interaction is one of the reasons due to which the depth of the fusion pocket decreases in the effective potential-energy curve. So, the absence of the fusion pocket may lead to the breakup of the incident nucleus into its constituents. Since, the strength of the Coulomb interaction between the interacting partners, with the projectile of charge Z_P and the target of charge Z_T, is proportional to the $Z_P Z_T$, hence, it will be interesting to investigate the role of the $Z_P Z_T$, called the Coulomb factor, on the ICF reactions.

In addition the magnitude of the critical angular-momentum ℓ_{crit} also decreases with the increase of $Z_P Z_T$ [17]. If an incident nucleus reaches the region of the fusion pocket, it will be trapped in the pocket resulting in the fusion of the incident and target nuclei. Thus, for a given incident energy and at an impact parameter $b < \ell_{crit}$, the incident and the target nuclei will have a *finite probability* of getting trapped in the potential minimum (fusion pocket) for sufficiently long time, enough to form a compound nucleus. And, this *probability* increases with the depth and the width of the fusion pocket.

Hence, to understand the $Z_P Z_T$ dependence of the ICF reactions, the measured ICF strengths of the present system have been compared with the low-energy ICF data available, for a large number of ($\approx$45) projectile-target combinations with $Z_P Z_T$ spanning a wide range $\approx$138–670 from the literature. Thus, the F_{ICF} values at a constant normalized projectile energy, say at $E_{lab}/V_b \approx 1.35$, have been plotted as a function of $Z_P Z_T$ in Fig. 7. One can clearly notice from this figure that the F_{ICF} values for all these systems are not advocates any systematic trend. Although, a broad linear increasing trend of F_{ICF} values with $Z_P Z_T$ can be noticed, which reflects that as the projectile comes close to the target nucleus, the weight of the Coulombic interaction increases, consequently, the breakup probability of the projectile also increases, which followed by fusion of one or more of the constituent fragments with the target nuclei. Therefore, it may be concluded that as the value of $Z_P Z_T$ increases, the strength of the Coulomb interaction also enhances, leading to the more breakup probability of the projectile.

Furthermore, it is not out of place to mention on the basis of this figure that, despite having same or almost same $Z_P Z_T$ values for some systems, their ICF contributions are
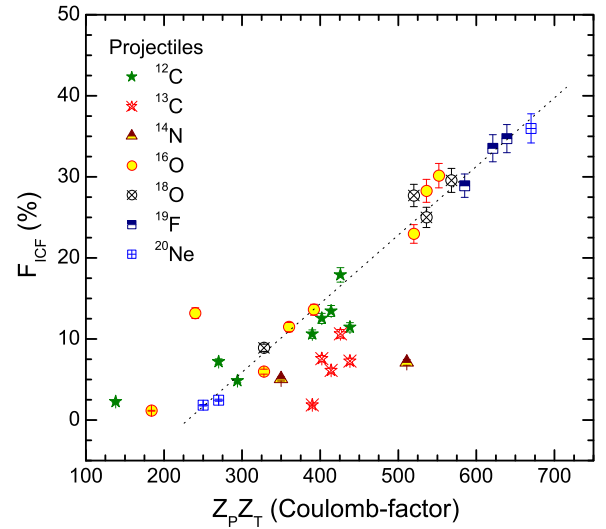

FIG. 7. The comparison of the incomplete fusion fraction F_{ICF} with Coulomb-factor $Z_P Z_T$ for all the systems (see text for the explanation).

considerably different. And this observation could not be understood through the Coulomb-factor systematics only. Few systems with similar $Z_P Z_T$ values are marked by A, B, C, D, etc., in Table I. For all these systems, different trends of F_{ICF} have been observed, and an attempt has been made to explain the magnitude of F_{ICF} for such systems on the basis of the Q_α value of the projectile or the mass asymmetry of the interacting partners in Ref. [35]. For example, systems ^{16}O + ^{159}Tb and ^{18}O + ^{159}Tb having same $Z_P Z_T$ value of 520, however, their ICF contributions are widely different in the entire range of studied energy. The ^{18}O as projectile on ^{159}Tb having more incomplete fusion contribution than the ^{16}O projectile on the same target. This difference in ICF's magnitude can be understood on the basis of the projectile's Q_α value, as for the ^{16}O + ^{159}Tb system the Q_α value of the projectile ^{16}O is more negative than the ^{18}O as projectile in the system ^{18}O + ^{159}Tb, thus leads to a lower breakup probability. Similar observations have also been noticed for the other projectile-target combinations with the same $Z_P Z_T$ values and have been explained by considering the projectile's Q_α value.

Hence, based on these observations it can be understood that, for systems with the same or almost the same $Z_P Z_T$ values, the ICF contribution is decided by the Q_α value of the projectile or the mass-asymmetry of the interacting partners. Thus, the Coulomb effect systematics, i.e., the $Z_P Z_T$ factor, alone is not the effective parameter to understand the low-energy ICF data, consequently, other entrance channel parameters like the Q_α value of the projectile or the mass asymmetry of the colliding partners also plays an important role to understand the low-energy ICF-reaction dynamics.

F. Attempts for some general systematics

It has been established from the previous discussion that most of the low-energy ICF's dependence on these various entrance channel parameters, whether it is the entrance channel mass-asymmetry (α_{mass}) or the Coulomb factor $Z_P Z_T$ or
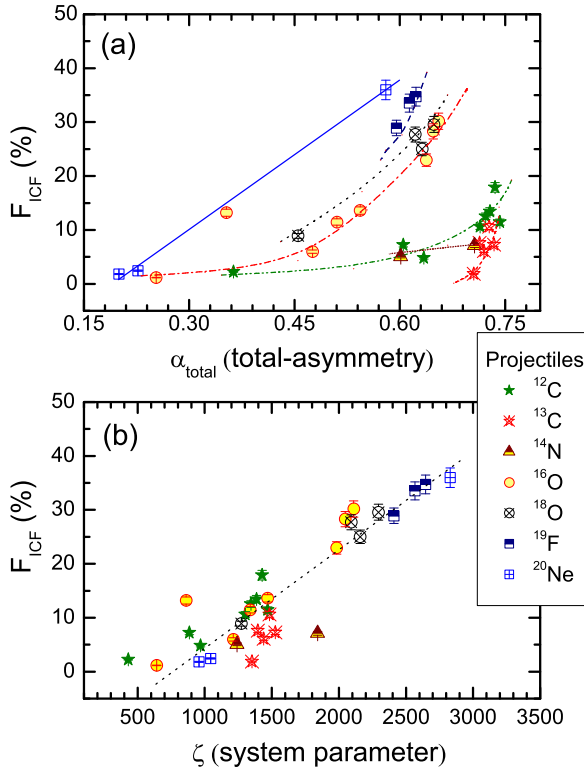
FIG. 8. The incomplete fusion fraction F_{ICF} for various systems have compared in terms of (*a*) the total asymmetry parameter α_{total}, (*b*) the system parameter (ζ) (see text for the explanation).

the fissility parameter, hints for a projectile dependency along with these parameters. Hence, attempts have been made to understand this dependence of the low-energy ICF reactions through some general parameters, which should include both the mass and charge dependency of these reactions. The details of the systematics are given in the following sections:

1. Role of total asymmetry parameter α_{total}

The mass-asymmetry dependence of the ICF fraction has been discussed in the previous Sec. IV B, which hints for some projectile type dependency of the ICF reactions, as different trends of the ICF fractions have been observed for different types of projectiles. Thus, to incorporate the projectile type dependence along with the mass dependence of the ICF reactions, a parameter called the total asymmetry parameter (α_{total}), which is defined as the total asymmetry in mass and charge of the interacting partners, i.e.; $\alpha_{total} = \alpha_{mass}\alpha_{charge}$, where mass asymmetry is already defined in previous Sec. IV B as $\alpha_{mass} = (A_T - A_P)/(A_T + A_P)$, and similarly the charge asymmetry is also defined as; $\alpha_{charge} = (Z_T - Z_P)/(Z_T + Z_P)$, and the symbols have their usual meanings.

Hence, the F_{ICF} values, at a constant E_{lab}/V_b value (≈ 1.35) for all the studied systems, have been plotted with respect to the α_{total} in Fig. 8(a). As it is clearly visible from this Fig. 8(a) that, even after including the projectile type dependency through the charge asymmetry parameter α_{charge} in the total asymmetry parameter α_{total}, the F_{ICF} trends have not

changed much from the Fig. 5. Still, the different F_{ICF} trends have indicates some projectile-type dependency. Thus, it can be concluded that the total asymmetry parameter does not suit well to unify the dependencies of the low-energy ICF reactions.

2. Role of system parameter ζ

In the previous section IV E, we have discussed the $Z_P Z_T$ dependence and concluded that the Coulomb interaction may play a role in the fragmentation of the projectile. Apart from this the limitations of the $Z_P Z_T$ systematics have also been discussed in the same section. Now, since the semiclassical or classical approaches are more appropriate and successful, when the large angular momentum and smaller wavelengths are involved. Also, the semiclassical treatment is applicable whenever the Sommerfeld parameter is much larger than the unity, and for the systems of the low-energy ICF data, the values of the Sommerfeld parameter are ranging from ≈ 10–40, consequently the semiclassical treatment can be applied to understand the reaction dynamics. The Sommerfeld parameter is defined as

$$\eta = \frac{Z_P Z_T e^2}{4\pi\epsilon_o \hbar v}. \tag{1}$$

The symbols have their usual meanings. The relative velocity v can be written as $v = \sqrt{2E_{CM}}/\sqrt{\mu}$. Thus, the Sommerfeld parameter can be rewritten as

$$\eta = 0.1575 \star Z_P Z_T \sqrt{\frac{\mu}{E_{CM}}}, \tag{2}$$

where μ [$=A_P A_T/(A_P + A_T)$] is the reduced mass of the system. The Sommerfeld parameter can now be written like this:

$$\eta = \frac{0.1575 \star \zeta}{\sqrt{E_{CM}}}. \tag{3}$$

Here in this equation (3), the symbol ζ ($=Z_P Z_T \sqrt{\mu}$) is called the "system parameter." Hence, in order to see the ICF's dependency on this system parameter, which seems to be more general parameter (because it incorporates the Coulomb factor as well as the masses of the interacting partners) in comparison to the previously discussed parameters, the values of F_{ICF} for different systems have been plotted against the system parameter ζ at a constant E_{lab}/V_b in Fig. 8(b). It may clearly be seen from this figure that there is a broad linear dependence of the ICF fraction on the system parameter ζ, almost for all the systems, the ICF fraction increases as the system parameter increases. However, in previous section (IV E) of $Z_P Z_T$ systematics, significant role of the projectile type was clearly visualized, and the difference in the values of the ICF fraction at the same $Z_P Z_T$ values were understood on the basis of Q_α values of the projectile. Now, in this Fig. 8(b) that effect of the Q_α value on the ICF fraction, almost for all the projectiles, is following the same increasing trend with the system parameter ζ. But, the data points for ^{13}C, and ^{14}N as projectiles on different targets have little, visible, deviation in the ICF values from the over all trend. It is not out of place to mention that the Q_α value for ^{13}C (-10.76), and

^{14}N (-11.61 MeV) having more negative Q_α values than the other projectiles. Consequently, the effect of the Q_α value for ^{13}C and ^{14}N could not be smeared out by the $\sqrt{\mu}$ factor of the system parameter. However, the Q_α values for the other projectiles are nearby to each other, thus taken care well in the system parameter of the interacting partners. This concludes that the system parameter explains the low-energy ICF data more clearly than the other parameters.

V. SUMMARY

The present article reports the EFs measurements of several evaporation residues populated in the interactions of ^{18}O on ^{159}Tb target nuclei, in the energy range $1.01V_b$ to $1.42V_b$. In these measurements the activation technique along with the off-line γ-ray spectroscopy have been used. To understand their production mechanism, the experimentally measured EFs have been analyzed using the PACE4 code, which is a statistical model code based on the compound nucleus hypothesis. The analysis of the experimentally measured EFs of the xn channels concludes that the production mechanism of these residues are mainly through the CF reaction processes, because a reasonably well reproduction of experimentally measured EFs of xn channels with the predictions of statistical model code PACE4 (done with level density parameter $a = A/8$ MeV^{-1}) have been observed. In the present work none of the pxn channels could be observed, may be due to their short and long half-lives. However, their contribution to the total fusion cross section have been estimated (which is less than 2%–3% over the studied energy range) using the PACE4 calculations and same have been incorporated while deducing the ICF strength function. Furthermore, the experimentally measured EFs for all the α-emitting channels shows notable enhancement as compared with the PACE4 predictions (performed with the same set of parameters as has been used to explain the xn channels). This enhancement in the production cross section of α-emitting channels may be assign to the contribution of ICF reaction processes. It is not out of place to mention that the PACE4 code does not include the contribution for pre-equilibrium and ICF reactions into account.

Furthermore, the ICF contribution, enhancement over the PACE4 predictions have been deduced at each studied energy for the present system. This method of deducing strength of ICF reactions is subject to model calculations. Nevertheless, this procedure of deducing the ICF contribution agree reasonably well with that of the model independent approaches of calculating the ICF strengths, like; the measurement of forward recoil ranges, angular distributions, where CF and ICF contributions deduced independently through respective events. Furthermore, the CF contribution, in the production of α-emitting channels, measured in the recoil range distribution measurements, where the CF and ICF contributions have been measured distinctly based on the full and fractional linear momentum transfer components, has satisfactorily matches with the predictions of the PACE4 calculations done with the level-density parameter $a = A/8$ MeV^{-1}. This match certainly validate the values of PACE4 parameters used in such analysis, and of course, give confidence to the present method of deducing the ICF contribution.

Moreover, the ICF strength have been deduced for the present system and compared with the low-energy ICF data available in the literature. The analysis indicates some strong dependence of ICF strength function on entrance channel parameters, such as on the incident beam energy, the mass asymmetry, fissility, Q_α value of the projectile, and also on the Coulomb factor. The dependence of ICF fraction on the mass asymmetry, fissility, and $Z_P Z_T$ show a strong projectile-type dependency, which inarguably explained with the inclusion of the Q_α value of the projectile. In the present work, in order to achieve better understanding on the dependence of low-energy incomplete fusion reaction dynamics on various entrance channel parameters, first time we have compared the low-energy ICF data for about $\approx$45 different projectile-target combinations with $Z_P Z_T$ values spanning a wide range of 138–670. Furthermore, in the present work an attempt has been made to find out a more general parameter, which should include the charge and mass dependency of the ICF reactions. In this regard, two parameters, (i) the total asymmetry parameter α_{total}, and (ii) the system parameter ζ have been attempted to explain the low-energy ICF data. It has been concluded that the *system parameter* ζ, which includes the Coulomb factor ($Z_P Z_T$) as well as the mass dependence of the interacting partners, seems a reasonably good parameter to understand the ICF reaction dynamics at such low energies. Although for large Q_α values, the ICF data deviate from the systematics and thus we need to explore the possibility of a more general parameter or a reduction methodology which can segregate the different weights of the entrance channel parameters.

[1] A. C. Berriman *et al.*, Nature (London) **413**, 144 (2001).

[2] S. Hofmann *et al.*, Eur. Phys. J. A **32**, 251 (2007); **14**, 147 (2002).

[3] R. N. Sagaidak, M. L. Chelnokov, V. I. Chepigin, V. A. Gorshkov, O. N. Malyshev, A. G. Popeko, A. I. Svirikhin, and A. V. Yeremin, Phys. Rev. C **105**, 024604 (2022).

[4] V. I. Zagrebaev, Nucl. Phys. A **734**, 164 (2004).

[5] B. B. Back, H. Esbensen, C. L. Jiang, and K. E. Rehm, Rev. Mod. Phys. **86**, 317 (2014).

[6] L. Corradi *et al.*, Nucl. Phys. A **734**, 237 (2004).

[7] Yu. Ts. Oganessian *et al.*, Nature (London) **400**, 242 (1999), and references therein.

[8] M. Lefort, Rep. Prog. Phys. **39**, 129 (1976).

[9] M. Dasgupta *et al.*, Nucl. Phys. A **787**, 144 (2007); **734**, 148 (2004).

[10] P. R. S. Gomes *et al.*, Phys. Rev. C **73**, 064606 (2006); Phys. Lett. B **601**, 20 (2004).

[11] R. I. Badran *et al.*, Eur. Phys. J. A **12**, 317 (2001).

[12] H. C. Britt and A. R. Quinton, Phys. Rev. **124**, 877 (1961).

[13] J. M. Alexander and L. Winsberg, Phys. Rev. **121**, 529 (1961).

[14] H. Morgenstern, W. Bohne, W. Galster, K. Grabisch, and A. Kyanowski, Phys. Rev. Lett. **52**, 1104 (1984); H. M. Morgenstern *et al.*, Z. Phys. A **313**, 39 (1983); Phys. Lett. B **113**, 463 (1982).

[15] T. Udagawa and T. Tamura, Phys. Rev. Lett. **45**, 1311 (1980); Phys. Lett. B **116**, 311 (1982).

[16] E. Takada, T. Shimoda, N. Takahashi, T. Yamaya, K. Nagatani, T. Udagawa, and T. Tamura, Phys. Rev. C **23**, 772 (1981).

[17] J. Wilczynski, K. Siwek-Wilczynska, J. vanDriel, S. Gonggrijp, D. C. J.M. Hageman, R. V. F. Janssens, J. Lukasiak, and R. H. Siemssen, Phys. Rev. Lett. **45**, 606 (1980); J. Wilczynski *et al.*, Nucl. Phys. A **373**, 109 (1982).

[18] M. Blann, Phys. Rev. Lett. **27**, 337 (1971).

[19] J. P. Bondorf *et al.*, Nucl. Phys. A **333**, 285 (1980).

[20] B. G. Harvey, Phys. Lett. B **130**, 373 (1983); Nucl. Phys. A **444**, 498 (1985).

[21] A. Y. Abul-Magd, Z. Phys. A: At. Nucl. **298**, 143 (1980).

[22] M. H. Simbel and A. Y. Abul-Magd, Z. Phys. A: At. Nucl. **294**, 277 (1980).

[23] A. Diaz-Torres, D. J. Hinde, J. A. Tostevin, M. Dasgupta, and L. R. Gasques, Phys. Rev. Lett. **98**, 152701 (2007).

[24] A. Diaz-Torres and I. J. Thompson, Phys. Rev. C **65**, 024606 (2002).

[25] E. Z. Buthelezi *et al.*, Nucl. Phys. A **734**, 553 (2004).

[26] J. O. Newton *et al.*, Phys. Lett. B **586**, 219 (2004).

[27] P. P. Singh, B. P. Singh, M. K. Sharma, Unnati, D. P. Singh, R. Prasad, R. Kumar, and K. S. Golda, Phys. Rev. C **77**, 014607 (2008), and references therein.

[28] I. M. Bhat *et al.*, Nucl. Phys. A **1021**, 122421 (2022).

[29] M. S. Asnain *et al.*, Phys. Rev. C **104**, 034616 (2021).

[30] R. Rafiei, R. du Rietz, D. H. Luong, D. J. Hinde, M. Dasgupta, M. Evers, and A. Diaz-Torres, Phys. Rev. C **81**, 024601 (2010).

[31] L. R. Gasques, D. J. Hinde, M. Dasgupta, A. Mukherjee, and R. G. Thomas, Phys. Rev. C **79**, 034605 (2009).

[32] D. J. Hinde, M. Dasgupta, B. R. Fulton, C. R. Morton, R. J. Wooliscroft, A. C. Berriman, and K. Hagino, Phys. Rev. Lett. **89**, 272701 (2002).

[33] A. Yadav, V. R. Sharma, P. P. Singh, R. Kumar, D. P. Singh, Unnati, M. K. Sharma, B. P. Singh, and R. Prasad, Phys. Rev. C **86**, 014603 (2012).

[34] M. Shuaib *et al.*, Phys. Rev. C **94**, 014613 (2016).

[35] A. Yadav *et al.*, Phys. Rev. C **96**, 044614 (2017).

[36] P. K. Giri *et al.*, Phys. Rev. C **100**, 054604 (2019).

[37] A. Mahato *et al.*, Eur. Phys. J. A **56**, 131 (2020).

[38] P. K. Giri *et al.*, Phys. Rev. C **100**, 024621 (2019).

[39] H. Kumar *et al.*, Phys. Rev. C **99**, 034610 (2019).

[40] H. Kumar *et al.*, Eur. Phys. J. A **54**, 47 (2018).

[41] The Stopping and Range of Ions in Matter (SRIM) code: http://www.srim.org/SRIM/SRIMLEGL.htm.

[42] N. G. Puttaswamy *et al.*, Proceedings of DAE Symposium **34B** (1991).

[43] B. P. Ajith Kumar *et al.*, CANDLE: Collection and Analysis of Nuclear Data using Linux nEtwork (DAE **SNP**, Kolkotta, 2001).

[44] Unnati *et al.*, Nucl. Phys. A **811**, 77 (2008).

[45] K. Nishio *et al.*, Phys. Rev. Lett. **93**, 162701 (2004).

[46] E. Browne and R. B. Firestone, *Table of Radioactive Isotopes* (Wiley, New York, 1986).

[47] *Table of Isotopes*, 8th ed., edited by R. B. Firestone and V. S. Shirley (Wiley, New York, 1996).

[48] A. Gavron, Phys. Rev. C **21**, 230 (1980).

[49] O. B. Tarasov and D. Bazin, Nucl. Instrum. Methods Phys. Res., Sect. B **204**, 174 (2003).

[50] N. Bohr, Nature (London) **137**, 344 (1936).

[51] W. Hauser and H. Feshbach, Phys. Rev. **87**, 366 (1952).

[52] S. K. Kataria, V. S. Ramamurthy, and S. S. Kapoor, Phys. Rev. C **18**, 549 (1978).

[53] P. M. Endt, At. Data Nucl. Data Tables **26**, 47 (1981).

[54] R. Bass, Phys. Rev. Lett. **39**, 265 (1977); Nucl. Phys. A **231**, 45 (1974).

[55] A. Gilbert and A. G. W. Cameron, Can. J. Phys. **43**, 1446 (1965).

[56] U. Gupta *et al.*, Phys. Rev. C **80**, 024613 (2009).

[57] D. P. Singh *et al.*, Phys. Rev. C **81**, 054607 (2010).

[58] A. Yadav *et al.*, Phys. Rev. C **85**, 034614 (2012); **85**, 064617 (2012).

[59] A. Fleury and J. Alexander, Annu. Rev. Nucl. Sci. **24**, 279 (1974).

[60] S. Agarwal *et al.*, Z. Phys. A: At. Nucl. **296**, 287 (1980).

[61] M. Ismail *et al.*, Pramana **49**, 623 (1997).

[62] F. K. Amanuel, B. Zelalem, A. K. Chaubey, A. Agarwal, I. A. Rizvi, A. Maheshwari, and T. Ahmed, Phys. Rev. C **84**, 024614 (2011).

[63] A. Agarwal *et al.*, Int. J. Mod. Phys. E **17**, 393 (2008).

[64] B. B. Kumar, A. Sharma, S. Mukherjee, S. Chakrabarty, P. K. Pujari, B. S. Tomar, A. Goswami, S. B. Manohar, and S. K. Datta, Phys. Rev. C **59**, 2923 (1999).

[65] S. Mukherjee *et al.*, Int. J. Mod. Phys. E **15**, 237 (2006).

[66] S. Gupta, B. P. Singh, M. M. Musthafa, H. D. Bhardwaj, and R. Prasad, Phys. Rev. C **61**, 064613 (2000).

[67] P. P. Singh *et al.*, J. Phys.: Conf. Ser. **590**, 012031 (2015).

[68] H. Kumar *et al.*, Nucl. Phys. A **960**, 53 (2017).

[69] K. S. Babu *et al.*, J. Phys. G **29**, 1011 (2003).

[70] A. Agarwal *et al.*, Phys. Rev. C **105**, 034609 (2022).

[71] S. Tali *et al.*, Nucl. Phys. A **970**, 208 (2018).

[72] V. R. Sharma *et al.*, Phys. Rev. C **89**, 024608 (2014).

[73] R. Kumar *et al.*, Phys. Rev. C **96**, 054614 (2017).

[74] D. Singh *et al.*, J. Phys. Soc. Jpn. **82**, 114201 (2013).

[75] M. Kumar, A. Agarwal, S. Prajapati, K. Kumar, S. Dutt, I. A. Rizvi, R. Kumar, and A. K. Chaubey, Phys. Rev. C **100**, 034616 (2019).

[76] S. Sodaye *et al.*, Pramana **66**, 985 (2006).

[77] A. Sharma *et al.*, J. Phys. G **25**, 2289 (1999).

[78] K. Kumar, T. Ahmad, S. Ali, I. A. Rizvi, A. Agarwal, R. Kumar, and A. K. Chaubey, Phys. Rev. C **88**, 064613 (2013).

[79] P. P. Singh *et al.*, Eur. Phys. J. A **34**, 29 (2007).

[80] K. Kumar, T. Ahmad, S. Ali, I. A. Rizvi, A. Agarwal, R. Kumar, K. S. Golda, and A. K. Chaubey, Phys. Rev. C **87**, 044608 (2013).

[81] H. Kumar *et al.*, J. Nucl. Phys. Mat. Rad. A **3**, 47 (2015).

[82] D. P. Singh *et al.*, Phys. Rev. C **80**, 014601 (2009).

[83] A. Agarwal *et al.*, Phys. Rev. C **103**, 034602 (2021).

[84] M. Gull, Ph.D. thesis, Aligarh Muslim University, Aligarh, 2020 (unpublished).

[85] H. Kumar, Ph.D. thesis, Aligarh Muslim University, Aligarh, 2017 (unpublished).

[86] M. Shuaib *et al.*, J. Phys. G **44**, 105108 (2017).

[87] M. Shuaib *et al.*, Phys. Rev. C **98**, 014605 (2018).

[88] S. Ali *et al.*, J. Mod. Phys. **05**, 2063 (2014).

[89] R. Ali *et al.*, J. Phys. G **37**, 115101 (2010).

[90] D. Singh, R. Ali, M. AfzalAnsari, B. S. Tomar, M. H. Rashid, R. Guin, and S. K. Das, Phys. Rev. C **83**, 054604 (2011); D. Singh *et al.*, Nucl. Phys. A **981**, 75 (2019).

[91] R. Ali *et al.*, Indian J. Pure App. Phys. **57**, 570 (2019).

[92] D. Singh *et al.*, Nucl. Phys. A **879**, 107 (2012).

[93] L. Rayleigh, Philos. Mag. **14**, 184 (1882).

[94] N. Bohr and J. Wheeler, Phys. Rev. **56**, 426 (1939).